RSC Advances

PAPER

View Article Online
View Journal | View Issue

Cite this: *RSC Adv.*, 2026, **16**, 5548

Insights into the colloidal and structural stability of Atezolizumab with nonpolar amino acid-based ionic liquids under multiple stresses: phase two

Bayan Alkhawaja, *[ab] Faisal Al-Akayleh, [a] Saifeddin Daadoue,[a] Nour Alkhawaja,[a] Ghayda AlDabet,[c] Jehad Nassereden,[d] Muna Bustami,[a] Nidal Qinna,[ac] Mayyas Al-Remawi[a] and Andrew G. Watts[b]

Monoclonal antibodies (mAbs) are susceptible to physical and chemical instabilities, which compromise their therapeutic efficacy and shelf life. This study investigates the potential of renewable choline-amino acid-based ionic liquids (Ch-AA ILs), specifically choline valinate (CV) and choline glycinate (CG), to enhance the stability of the aglycosylated IgG1 antibody, Atezolizumab (Amab). Amab was formulated in varying concentrations of the ionic liquids (ILs) and subjected to ambient, thermal (40–70 °C), and chemical (urea) stress conditions. Stability was assessed using Dynamic Light Scattering (DLS) to measure the hydrodynamic diameter (D_r), UV-visible spectroscopy to determine the Aggregation Index (AI), and Attenuated Total Reflectance-Fourier Transform Infrared spectroscopy (ATR-FTIR) to analyse the secondary structure. The results demonstrated that CV, particularly at a 30% w/w concentration, confers superior colloidal stability to Amab compared to both CG and a conventional Tris–HCl buffer. Under significant thermal stress (70 °C for 24 hours), the 30% CV formulation maintained minimal aggregation (AI ≤ 17), whereas Amab in Tris buffer underwent extensive aggregation (AI > 160). However, an MTT assay employed to assess the biological activity of the stabilised antibody yielded inconclusive results. The ILs themselves caused a pronounced, nonspecific increase in apparent cellular metabolic activity, indicating that the assay is unsuitable for evaluating these formulations and may overestimate cell viability. This work highlights the significant promise of the green and renewable solvent CV as a stabilising excipient, enhancing the colloidal and structural stability of mAbs.

Received 31st October 2025
Accepted 13th January 2026

DOI: 10.1039/d5ra08395h

rsc.li/rsc-advances

1 Introduction

The advent of monoclonal antibodies (mAbs) has created a significant impact on the pharmaceutical field, becoming fundamental and serving as a cornerstone in the treatment of several diseases, including different malignancies, autoimmune disorders, and infectious diseases.[1,2] Their exquisite specificity and targeted mechanisms of action have contributed to the steep growth of their industry, with significant expansion anticipated in the years to come.[3,4] Atezolizumab (Amab), a humanised IgG1 monoclonal antibody targeting programmed cell death ligand 1 (PD-L1), is an example of this class of therapeutics. It functions as an immune checkpoint inhibitor, restoring anti-cancer immunity by inhibiting PD-L1:PD-1 and PD-L1:B7.1 interactions.[5,6]

Belonging to biological drugs and being of proteinous nature, mAbs are susceptible to various physical and chemical instabilities. These vulnerabilities pose considerable challenges to their formulation, long-term storage, and overall shelf life.[7,8] These instabilities present as conformational modifications, including unfolding, colloidal aggregation, and chemical degradation processes, such as oxidation and deamidation.[7,8] Ultimately, any form of degradation inresults to compromised therapeutic effectiveness, increased immunogenicity, and unsatisfactory product safety and efficacy of the product.[9,10] For instance, Amab is an IgG1 antibody that lacks an oligosaccharide associated with its Fc portion.[11] This aglycosylation characteristic makes such antibodies more susceptible to aggregation and instability.[12] Thus, this inherent vulnerability highlights the critical need for stabilization approaches to maintain the consistent effectiveness of therapeutic monoclonal antibodies.

Given the concerning stability issues in biopharmaceuticals, the investigation of innovative excipients, environmentally friendly systems and techniques has garnered considerable

[a]*Faculty of Pharmacy and Medical Sciences, University of Petra, Amman 11196, Jordan. E-mail: bayan.alkhawaja@uop.edu.jo; ba436@bath.ac.UK*
[b]*Department of Life Sciences, University of Bath, Claverton Down, BA2 7AY, Bath, UK*
[c]*University of Petra Pharmaceutical Centre, Faculty of Pharmacy and Medical Sciences, Petra University, Amman 11196, Jordan*
[d]*Department of Pharmaceutical Technology & Cosmetics, Faculty of Pharmacy, Middle East University, Amman 11831, Jordan*

attention.[13] One of the most promising candidates is ionic liquids (ILs),[14] which possess unique physicochemical properties such as low vapor pressure, high thermal stability, and great versatility.[15,16] In comparison to conventional organic solvents, many ionic liquids (ILs) are often referred to as "green solvents" due to their biocompatibility and biodegradability, which can be derived from natural sources such as amino acids.[15,17] Despite the promise of ILs as "green solvents," their application is associated with significant complexities. While ILs could enhance the thermal stability of proteins by increasing their melting temperature, they may also compromise conformational stability, potentially leading to protein unfolding and aggregation, which is a major concern for drug safety and efficacy.[14]

Furthermore, the biocompatibility of these compounds is often misunderstood. At the same time, some natural-source ILs show promise; many are cytotoxic, and their toxicity is highly dependent on their specific chemical structure and concentration.[18] Therefore, the successful application of ILs is not a one-size-fits-all solution but rather requires a case-by-case analysis to identify the optimal IL and concentration that balances the enhancement of thermal stability with the preservation of a protein's functional integrity.[19] For example, choline chloride-based ILs were utilised to stabilise immunoglobulin G4 (IgG4) antibodies and found to reduce the protein aggregation propensity.[10]

Choline-based ILs (Ch-ILs) and amino acid-based ILs (AA-ILs) are distinguished as "third-generation ILs" due to their non-toxicity and great potential for use in pharmaceutical and biomedical applications, from drug delivery to protein stabilization.[20,21] Previous research has already highlighted the positive impact of choline-based deep eutectic solvents and ILs on improving the conformational and colloidal stability of IgG antibodies.[22] However, a comprehensive understanding of how the diverse amino acid anions within Ch-AA ILs, specifically non-polar AA-ILs, influence the stability and, critically, the biological activity of therapeutic mAbs, especially under various stress conditions, remains an area requiring further rigorous exploration. This knowledge gap is pivotal for the rational design of next-generation biopharmaceutical formulations.

This research aims to prepare and characterize the choline-amino acid-based ionic liquids choline valinate (CV) and choline glycinate (CG) and use them to stabilize the aglycosylated IgG1 antibody, namely, Amab. The study evaluated the antibody's stability under ambient, thermal, and chemical stress conditions, comparing the results with those obtained using a conventional Tris–HCl buffer. A key focus was to understand how the amino acid's functional group influences protein secondary and tertiary structures, thereby affecting stability. Furthermore, the research verified the retention of Amab's biological activity in the most promising formulations after thermal stress. This work highlights the potential of these ionic liquids to enhance antibody stability and informs the rational design of future biopharmaceutical formulations with improved stability.

2 Materials and methods

2.1 Materials

Choline chloride (ChCl) and potassium Hydroxide (KOH) pellets were purchased from Tokyo Chemical Industry Co., Ltd (TCI, Japan). L-Amino acids (valine and glycine) were purchased from Sigma-Aldrich Chemical Company (USA). HPLC-grade ethanol (EtOH) was purchased from VWR (USA). Atezolizumab (Tecentriq) was kindly given from Pharmaxo Scientific. Phosphate-buffered saline (PBS) was obtained from EuroClone® (Netherlands). Trypsin/EDTA was purchased from Biowest® (USA) and MTT was obtained from PhytoTech Labs (USA).

2.2 Ionic liquid synthesis

The ILs used in this study were synthesized following the procedure outlined by phase 1 study.[21,23] In summary, potassium hydroxide was first dissolved in ethanol, after which choline chloride was introduced into the solution. Immediately following this, the amino acid was dissolved in the same mixture. The reaction in eqn (1), between potassium hydroxide, choline chloride, and the amino acid, was carried out at a molar ratio of 1 : 1 : 1.05 and allowed to stir overnight. Subsequently, the precipitated potassium chloride was removed by filtration, and the water and ethanol were evaporated using a rotary evaporator. The resulting IL was then washed with acetonitrile to precipitate any residual unreacted amino acid, followed by filtration and evaporation in a vacuum oven. The samples were characterized by NMR (Fig. S1). The pH of the ILs were reported in phase 1 study.

$$\text{R-CHNH}_2\text{COOH} + \text{KOH} + \text{ChCl} \xrightarrow{\text{EtOH}} \text{R-CHNH}_2\text{COOCh} + \text{KCL} + \text{H}_2\text{O} \quad (1)$$

2.3 Preparation of Amab-IL

Atezolizumab 1200 mg (Tecentriq) powder was reconstituted in deionized water. The concentration of Amab was quantified by measuring its absorbance at 280 nm using a Thermo Scientific Multiskan™ Sky plate reader at room temperature. Before formulation, Amab was buffer-exchanged into deionized water using an ultra-centrifugal filter (10 k MWCO). IL formulations of Amab were prepared by mixing varying ratios of IL (30%, 50%, 70%, and 80%) to achieve a final Amab concentration of 5 mg mL^{-1} (Table 1).

Table 1 The prepared ILs and their structure, ratios and codes

Structure	Sample code	Composition
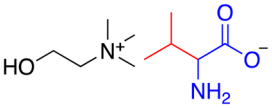	CV30	30% choline-valine IL
	CV50	50% choline-valine IL
	CV70	70% choline-valine IL
	CV80	80% choline-valine IL
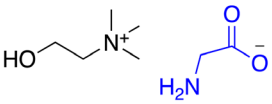	CG30	30% choline- glycine IL
	CG50	50% choline- glycine IL
	CG70	70% choline- glycine IL
	CG80	80% choline- glycine IL

Table 2 Average D_r and PDI for IL formulations, after incubation for 7 days at RT

	CV30 RT		CV50 RT		CV70 RT		CV80 RT	
	D_r	PDI	D_r	PDI	D_r	PDI	D_r	PDI
Day 0	11	0.458	12.6	0.58	12.62	0.774	15.06	0.639
Day 1	13	0.386	21.44	0.69	21.85	0.315	17.89	0.48
Day 4	14.29	1	49.49	0.4	50.61	0.382	15.27	0.349
Day 7	12.91	0.483	11.2	0.461	160.6	0.364	32.38	0.49

2.4 Stability

The colloidal and structural stability of Amab-IL formulations containing 30%, 50%, 70%, and 80% of the IL was evaluated using three analytical techniques: UV-visible spectroscopy, dynamic light scattering (DLS), and attenuated total reflectance-Fourier transform infrared spectroscopy (ATR-FTIR). A control sample of Amab was prepared in Tris–HCl buffer and included in all tests for comparison. Initial stability screening was conducted at room temperature over a period of 7 days to identify the most stable IL concentrations for further evaluation. Based on the colloidal and conformational performance under ambient conditions, selected formulations were subjected to thermal and chemical stress. For thermal testing, formulations were incubated at 40 °C, 50 °C, 60 °C, and 70 °C for defined time points of 3 hours and 24 hours to simulate accelerated storage conditions. To assess stability under chemical denaturation, additional samples were incubated with 3.5 M and 7 M urea at 50 °C for 1 hour. After each condition, aliquots were withdrawn and analyzed by DLS to determine hydrodynamic diameter (D_r) and polydispersity index (PDI), UV-visible spectroscopy to calculate the aggregation index (AI), and ATR-FTIR to evaluate secondary structure changes.

2.4.1 Measuring hydrodynamic diameter using DLS. Dynamic light scattering (DLS) was used to evaluate the propensity of the protein to aggregate in ILs. Measurements were taken using a Zetasizer Nano Series ZS (Malvern Instruments, UK) equipped with a 633 nm laser. Detection was achieved *via* a non-invasive back-scattering configuration at a fixed angle of 173°. Prior to measurement, 50 μL aliquots of each sample were diluted with deionized water to a standardized concentration of 0.5 mg mL^{-1}. Particle size distributions were determined through five replicate measurements, with each replicate consisting of 15 acquisition cycles. Samples were

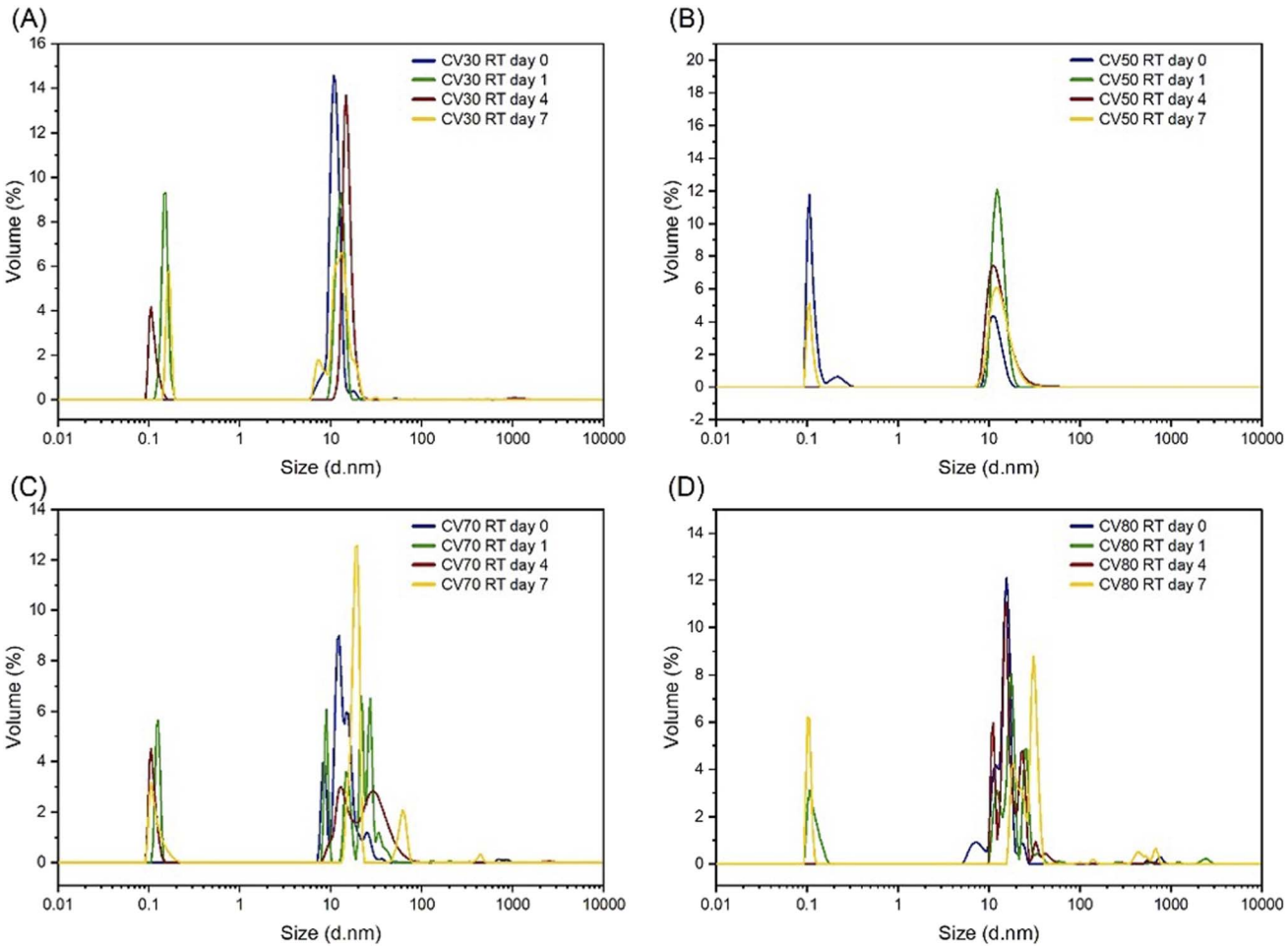

Fig. 1 Amab particle size distribution incubated in increasing ratio of CV ILs after incubation for 7 days at RT. (A) CV30, (B) CV50, (C) CV70 and (D) CV80.

Table 3 Average D_r and PDI for CG formulations, after incubation for 7 days at RT

	CG30 RT		CG50 RT		CG70 RT		CG80 RT	
	D_r	PDI	D_r	PDI	D_r	PDI	D_r	PDI
Day 0	11.92	0.603	10.42	0.484	11.76	0.339	12.11	0.462
Day 1	11.09	0.142	11.11	0.145	12.15	0.157	12.11	0.248
Day 4	13.29	0.281	20.12	0.524	13.71	0.345	47.19	0.395
Day 7	10.17	0.228	11.57	0.567	13.33	0.351	44.59	0.439

equilibrated for 30 minutes at 25 °C to ensure thermal stability prior to analysis. The D_r and PDI were derived from the measurements. The instrument employed cumulant analysis to compute the *z*-average diffusion coefficient and the PDI, the latter quantifying the extent of the size distribution. The D_r was computed from the diffusion coefficient (D) by applying the Stokes–Einstein equation, which considers the dispersant medium's viscosity and the calibration parameters specific to the instrument utilized.

2.4.2 UV-visible spectroscopy. Amab-IL samples were assessed for antibody aggregation by measuring their absorbance using a Thermo Scientific Multiskan™ Sky plate reader. The samples were injected into a μDrop plate, and the absorbance was measured within the 245 nm to 600 nm

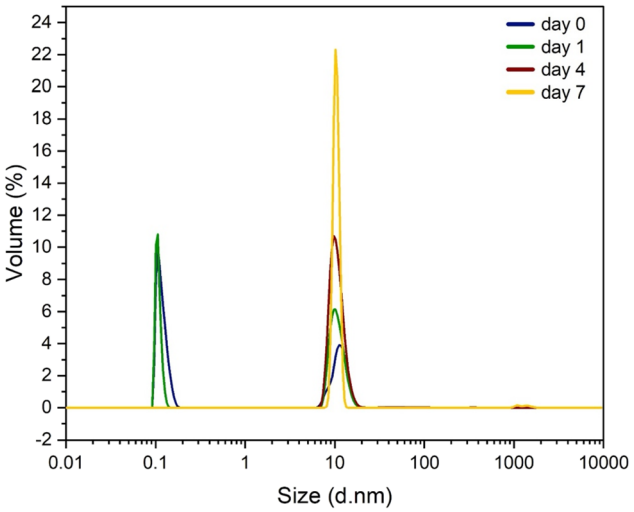

Fig. 3 Amab particle size distribution in incubated in Tris buffer after incubation for 7 days at RT.

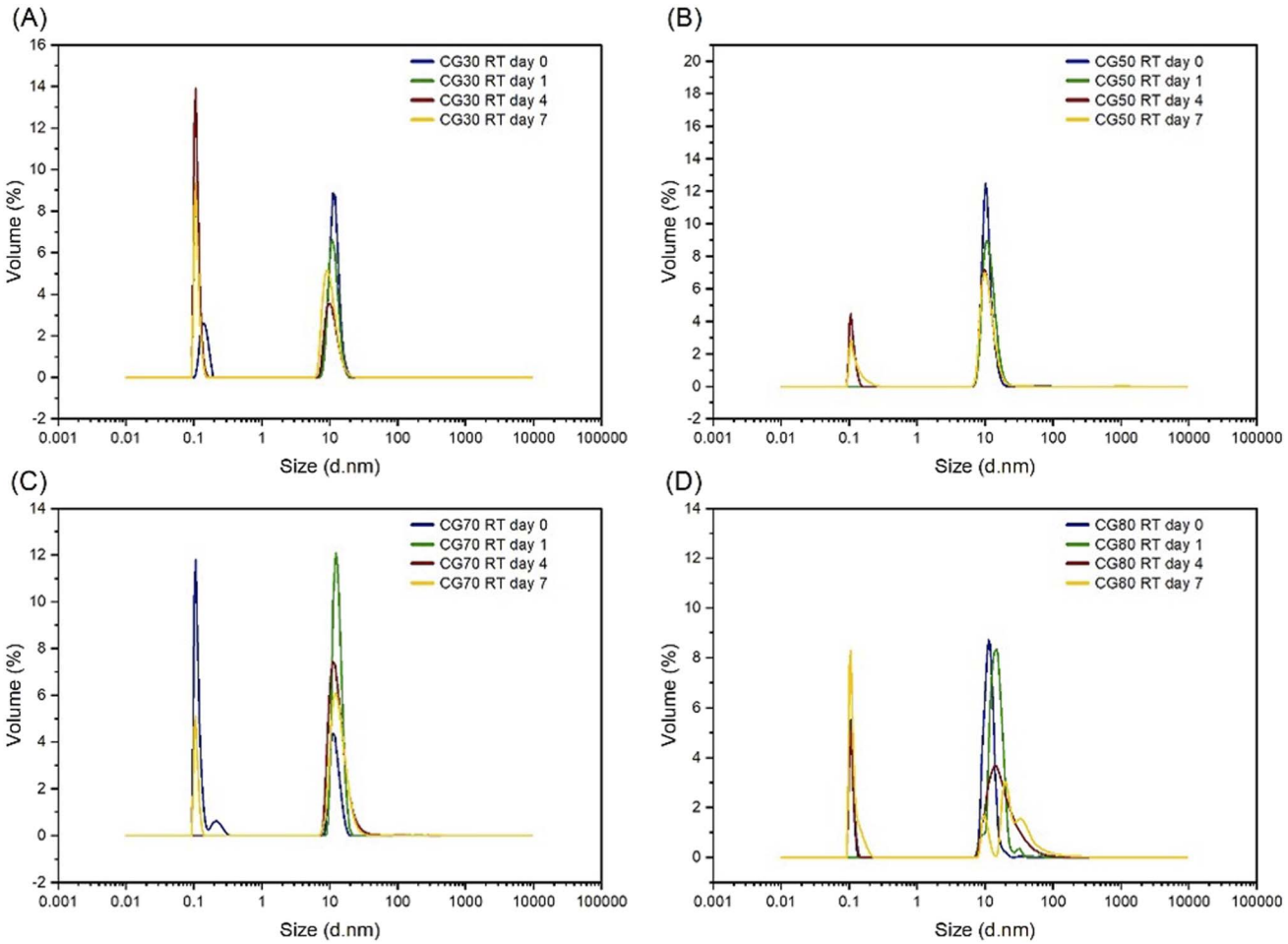

Fig. 2 Amab particle size distribution incubated in increasing ratio of CG ILs after incubation for 7 days at RT. (A) CG30, (B) CG50, (C) CG70 and (D) CG80.

Table 4 Calculated AI for Amab formulations at RT

	Zero-time RT	1 day RT	4 days RT	7 days RT
Tris buffer	10	10	16	15
CV30	17	14	16	17
CG30	27	32	40	44
CV50	17	16	22	23
CG50	33	37	51	58
CV70	19	26	26	27
CG70	36	40	49	57
CV80	19	24	19	25
CG80	39	43	56	60

wavelength spectrum. Samples were not subjected to any pre-processing procedures before analysis. The AI was determined using absorbance values at 280 nm and 340 nm, as indicated by eqn (2).

$$\mathrm{AI} = \frac{A340}{(A280 - A340)} \times 100 \quad (2)$$

2.4.3 Attenuated total reflectance – Fourier transform infrared spectroscopy (ATR – FTIR)

2.4.3.1 Freeze drying. The antibodies were dried using a Labconco FreeZone Benchtop Freeze Dryer (Labconco Co., Missouri, United States). The antibody samples were first stored in a −90 °C freezer overnight until frozen, then transferred to the freeze dryer. Freeze drying was carried out using a temperature of −50 °C and a vacuum pressure of 0 torr. Freeze-dried samples were then stored in a tightly sealed container at 4 °C.

ATR-FTIR spectra for both the freeze-dried and in-solution antibodies (reconstituted in 10 μL D_2O) were acquired using a PerkinElmer UATR Spectrum II (PerkinElmer, Massachusetts, United States) infrared spectrometer. Spectra were acquired in Absorbance mode across a wavenumber range of 4000 cm^{-1}–500 cm^{-1} using a resolution of 2 cm^{-1} and 32 scans per sample. The acquired spectra were then exported in comma-separated values (CSV). The CSV data was then imported into the Spectrogryph Spectroscopy Suite version 1.21.

2.5 Cell activity assay

EMT6/P cells (CRL-2755, ATCC) were maintained in high-glucose Dulbecco's Modified Eagle Medium (DMEM; Eurocl-one, Netherlands) supplemented with 10% heat-inactivated fetal bovine serum (FBS; Cytiva), 1% penicillin–streptomycin, 1% L-glutamine, and 1% non-essential amino acids. A 96-well plate was seeded with 1×10^5 cells per well and incubated under standard culture conditions (5% CO_2, 95% humidity, 37 °C) for 24 hours. Following incubation, cells were treated with

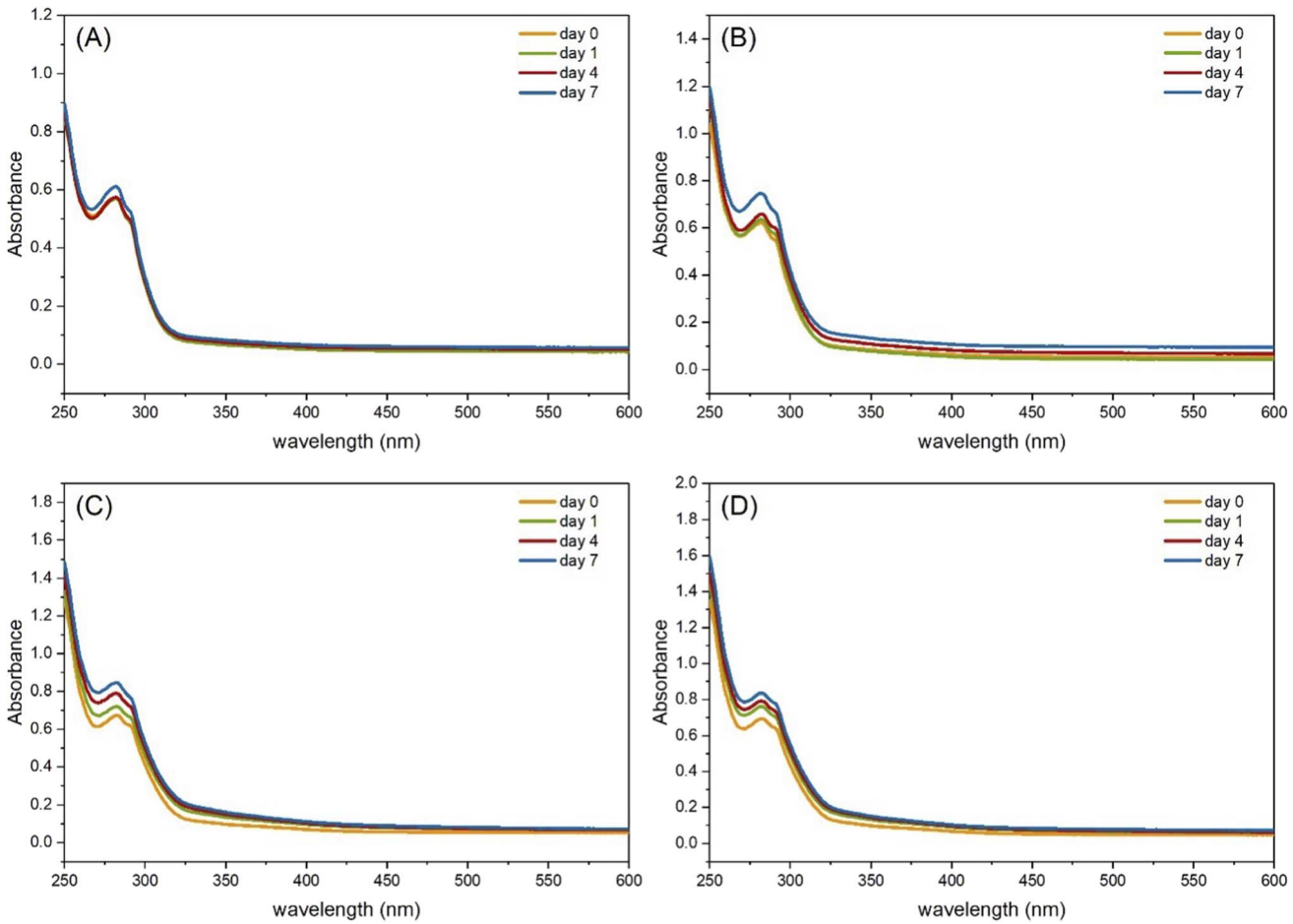

Fig. 4 UV-visible absorbance spectra of Amab IL formulations incubated at RT. (A) CV30 (B) CV50 (C) CV70 (D) CV80.

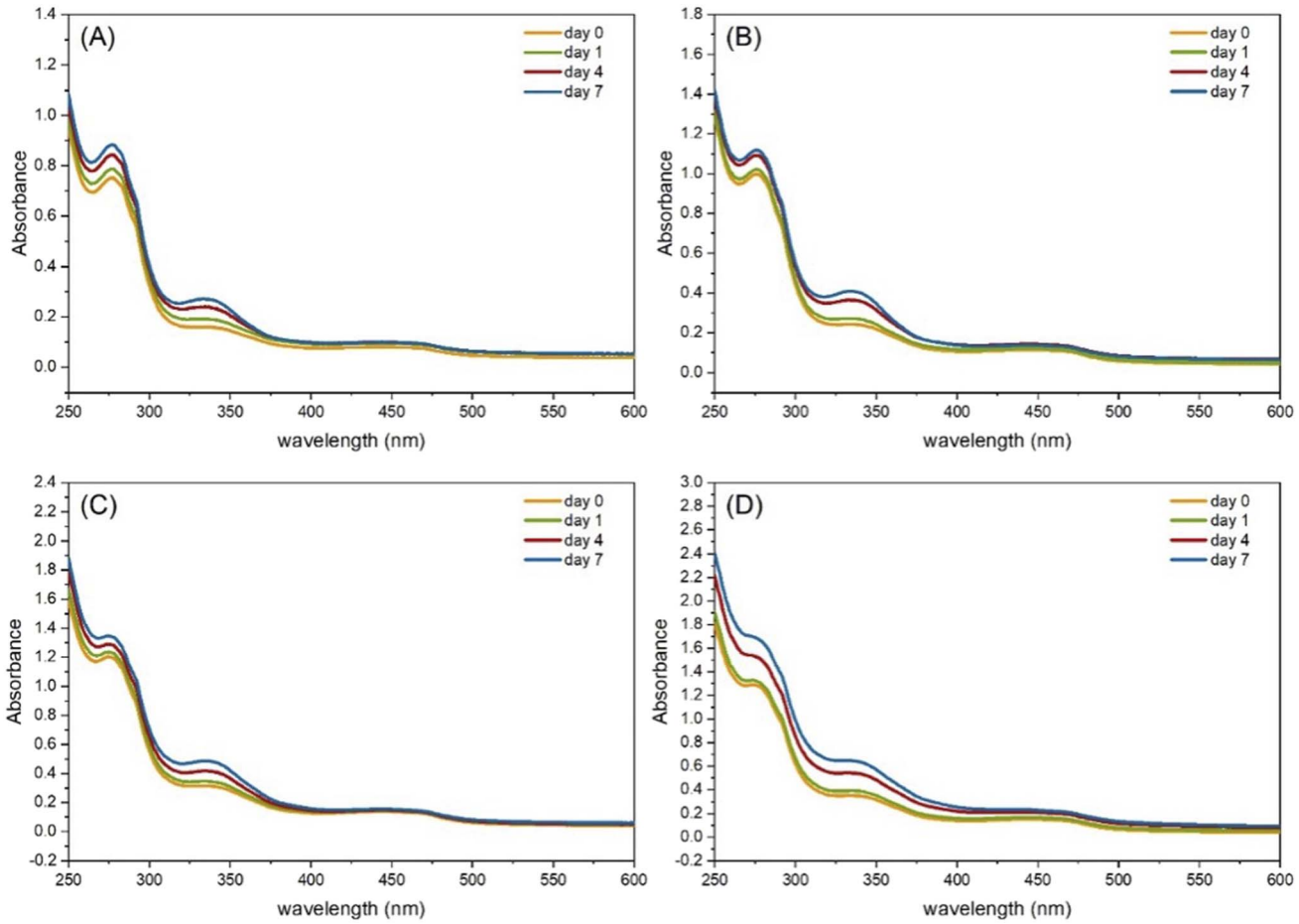

Fig. 5 UV-visible absorbance spectra of Amab IL formulations incubated at RT. (A) CG30 (B) CG50 (C) CG70 (D) CG80.

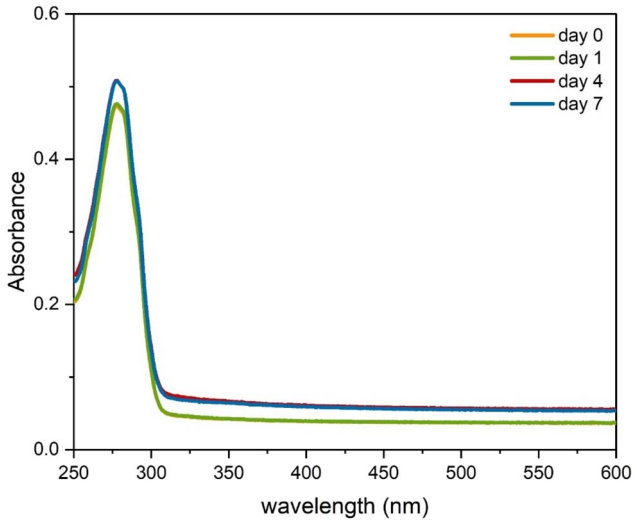

Fig. 6 UV-visible absorbance spectra of Amab in Tris buffer incubated at RT.

100 μL of Amab antibody to determine its IC_{50}. After 48 hours of exposure, cell activity was assessed using the MTT assay, as described by Alkhawaja *et al.*[21] (Fig. S2). Upon confirmation of the IC_{50} value for the Amab, control antibody, the assay was repeated using the various prepared formulations. The cell activity of the untreated control group was defined as 100% and used as a reference for calculating the relative absorbance of the treated samples.

3 Results

3.1 Study design

Previously, our group employed AA-ILs to stabilize therapeutic antibodies, where non-polar ILs (AA-ILs) were found optimal in maintaining the structural and colloidal stability of therapeutic antibodies (phase 1).[21] This study aims to expand upon our prior findings and address the gap in understanding the optimal conditions and their effects on the thermal and chemical stability of therapeutic antibodies (phase 2).

The design of this work is to utilize valine and glycine-based ILs as non-polar amino acids and explore various ratios with antibodies to find the optimum ratio and subsequently utilize the optimum ratio in thermal and chemical stability studies using DLS and VIS-UV spectroscopy as colloidal stability indicators. Following this, a selected group of samples was tested using FTIR to assess their secondary structure and their biological activity using the MMT assay.

Table 5 Average D_r and PDI for CV formulations, after incubation at increasing temperatures

	CV30 40 °C		CV30 50 °C		CV30 60 °C		CV30 70 °C	
	D_r	PDI	D_r	PDI	D_r	PDI	D_r	PDI
3 h	15.5	0.589	16.2	0.411	31.83	0.262	40.02	0.313
24 h	55.37	0.656	32.24	0.578	36.32	0.905	339.3	0.95
	CV50 40°C		**CV50 50°C**		**CV50 60°C**		**CV50 70°C**	
3 h	51.32	0.522	61.24	0.323	22.4	0.352	21.4	0.744
24 h	89.97	0.732	48.09	0.538	28.3	0.745	421.3	0.358
	Tris buffer 40°C		**Tris buffer 50°C**		**Tris buffer 60°C**		**Tris buffer 70°C**	
3 h	10.31	1	10.7	0.899	9.77	0.851	1701	0.996
24 h	7.146	0.558	10.87	0.813	12.49	0.956	973.7	0.618

Table 6 Calculated AI for Amab formulations at increasing temperatures

	40 °C		50 °C		60 °C		70 °C	
	3 h	24 h	3 h	24 h	3 h	24 h	3 h	24 h
CV30	15	15	18	16	12	13	14	16
CV50	21	22	16	17	15	18	19	25
Tris buffer	15	12	14	14	24	49	48	161

3.2 Colloidal stability assessment

3.2.1 Stability at room temperature using various ratios of IL. Four formulations of increasing ratios of IL were prepared, ranging from 30% to 80%. The colloidal behavior of Amab-IL was evaluated using DLS, providing insight into the D_r and PDI. At room temperature, CV at 30% and 50% w/w maintained D_r in the monomeric range (~10–14 nm) over a period of 7 days, with moderate PDI values (<0.5), indicating colloidal stability. Notably, CV50 exhibited a decrease in size from 21.4 nm on day 1 to 11.2 nm by day 7 (PDI = 0.461), suggesting a possible reorganisation toward a monomeric state. Size exclusion chromatography, SDS-PAGE and other techniques are usually used to understand the change in hydrodynamic diameter and confirm the formation of monomers or other lower molecular weight species.[22] Previously, in the phase 1 study, SDS PAGE experiment confirmed that monomers are the main observed species.[21]

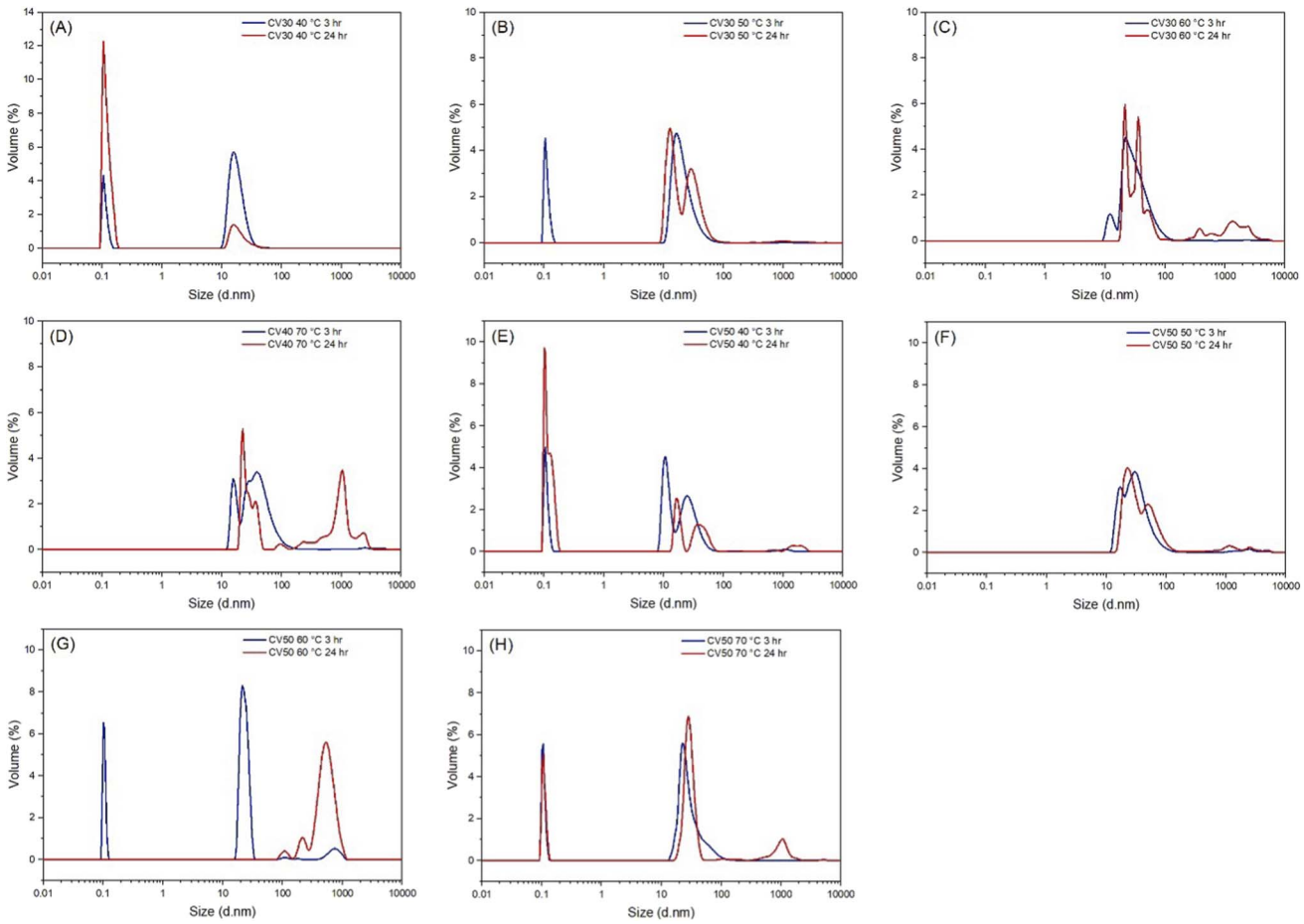

Fig. 7 Amab particle size distribution incubated in CV30 and CV50 ILs after incubation for 24 h at increasing temperatures ranging from 40 °C to 70 °C. (A) CV30 at 40 °C, (B) CV30 at 50 °C, (C) CV30 at 60 °C, (D) CV30 at 70 °C, (E) CV50 at 40 °C, (F) CV50 at 50 °C, (G) CV50 at 60 °C and (H) CV50 at 70 °C.

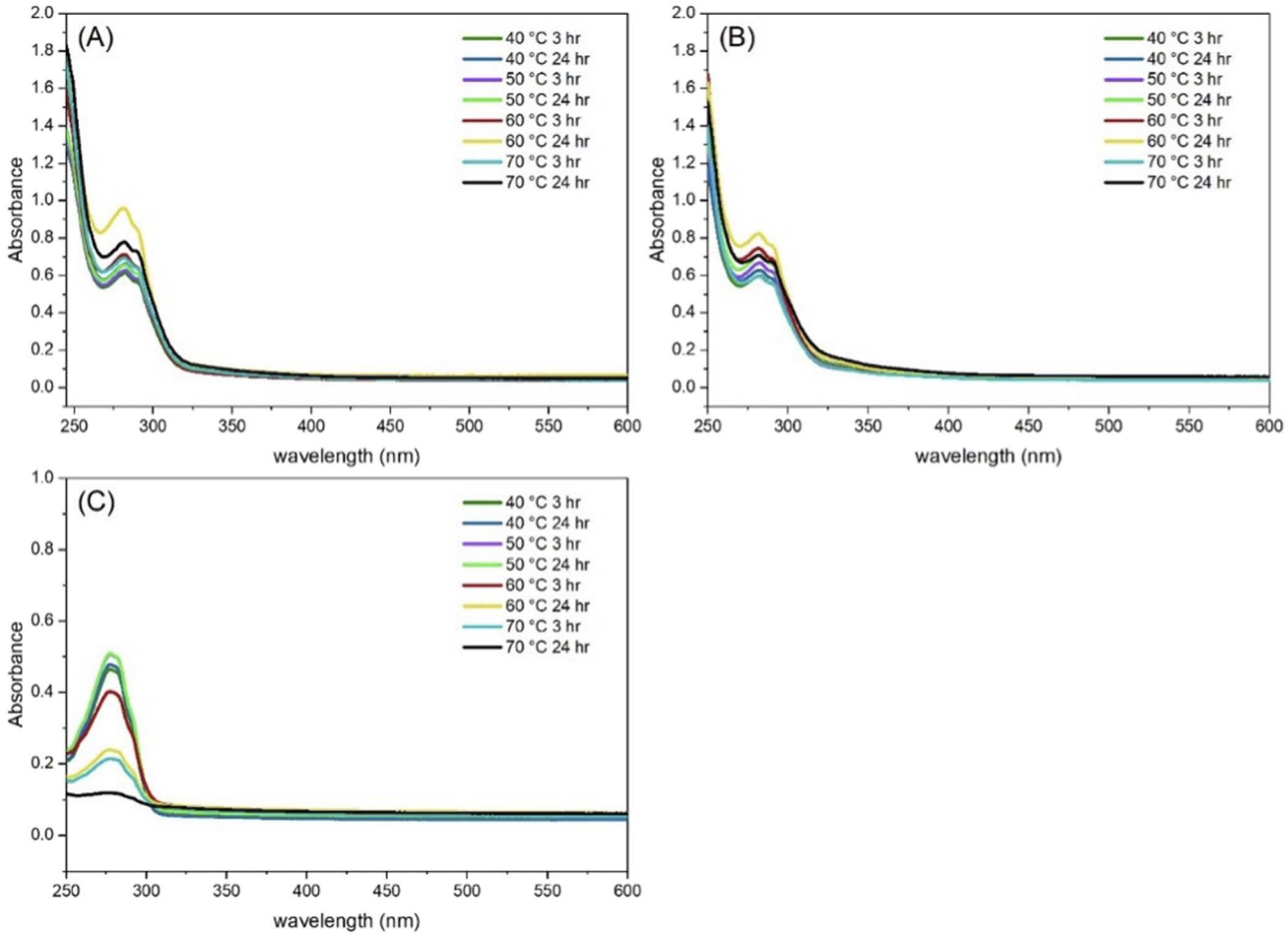

Fig. 8 UV-visible absorbance spectra of Amab formulations at increasing temperatures. (A) CV30 (B) CV50 (C) Tris buffer.

In contrast, higher concentrations of CV (70% and 80%) led to a sharp increase in size (up to 160.6 nm), indicating the formation of aggregates (Table 2, Fig. 1).

At RT, CG ILs showed favorable outcomes. The initial particle sizes (day 0) ranged from 10.4–12 nm across concentrations, with only minor increases observed over time, except for 80% w/w formulations, where sizes exceeded 50 nm by day 7. These increases coincided with PDIs near or above 0.5, suggesting increased polydispersity and aggregate formation (Table 3 and Fig. 2). It is worth noting that Amab in Tris buffer showed results comparable to CV30 IL, with D_r increasing over time (Fig. 3).

The AI, derived from UV-visible spectrophotometric data, was used to enhance the assessment of colloidal stability and identify subtle conformational changes. An AI value below 10 usually indicates low aggregation.[24,25] At room temperature, AI values for Amab in CV formulations were lower than those for CG, resulting in significantly lower aggregation. In particular, the AI values for CV30 remained below 17 for 7 days, indicating minimal increment of aggregation over time and consistent with stable DLS profiles. In contrast, the values for CG formulations increased significantly over time, especially at higher concentrations (50–80%), where the values surpassed 50 by day 4, indicating progressive aggregation (Table 4 and Fig. 4–6).

UV-visible spectroscopy enables the inference of conformational changes in proteins and the influence of ILs media on the tertiary structures of Amab, as evidenced by variations in λ_{max} (a peak at around 280 nm attributable to the response of aromatic residues). Shifts in λ_{max} may indicate protein unfolding or aggregation, resulting from changes in the microenvironments of the aromatic amino acids. To this end, Amab prepared in Tris buffer did not affect λ_{max} when incubated at RT for 7 days. Interestingly, the incubation with CV formations (30–80%) at RT did not cause any changes in the λ_{max}. In contrast, CG formations (30–80%) exhibited a hypsochromic shift, particularly after 7 days of incubation at RT (Fig. 4–6).

3.2.2 Thermal stability. Under thermal stress, CV30 formulation demonstrated superior stability, with D_r maintained below 17.7 nm and PDIs ≤0.589 after 3–24 h at 40–50 °C. Even at 60 °C and 70 °C, the size increase remained modest compared to Tris buffer (Fig. S3), in which the diameter increased sharply at ≥60 °C (up to 161 nm at 70 °C, 24 h), accompanied by a significant increase in polydispersity.

The standard melting temperature of IgG antibodies ranges between 60 and 70 °C, which explains the observed sharp

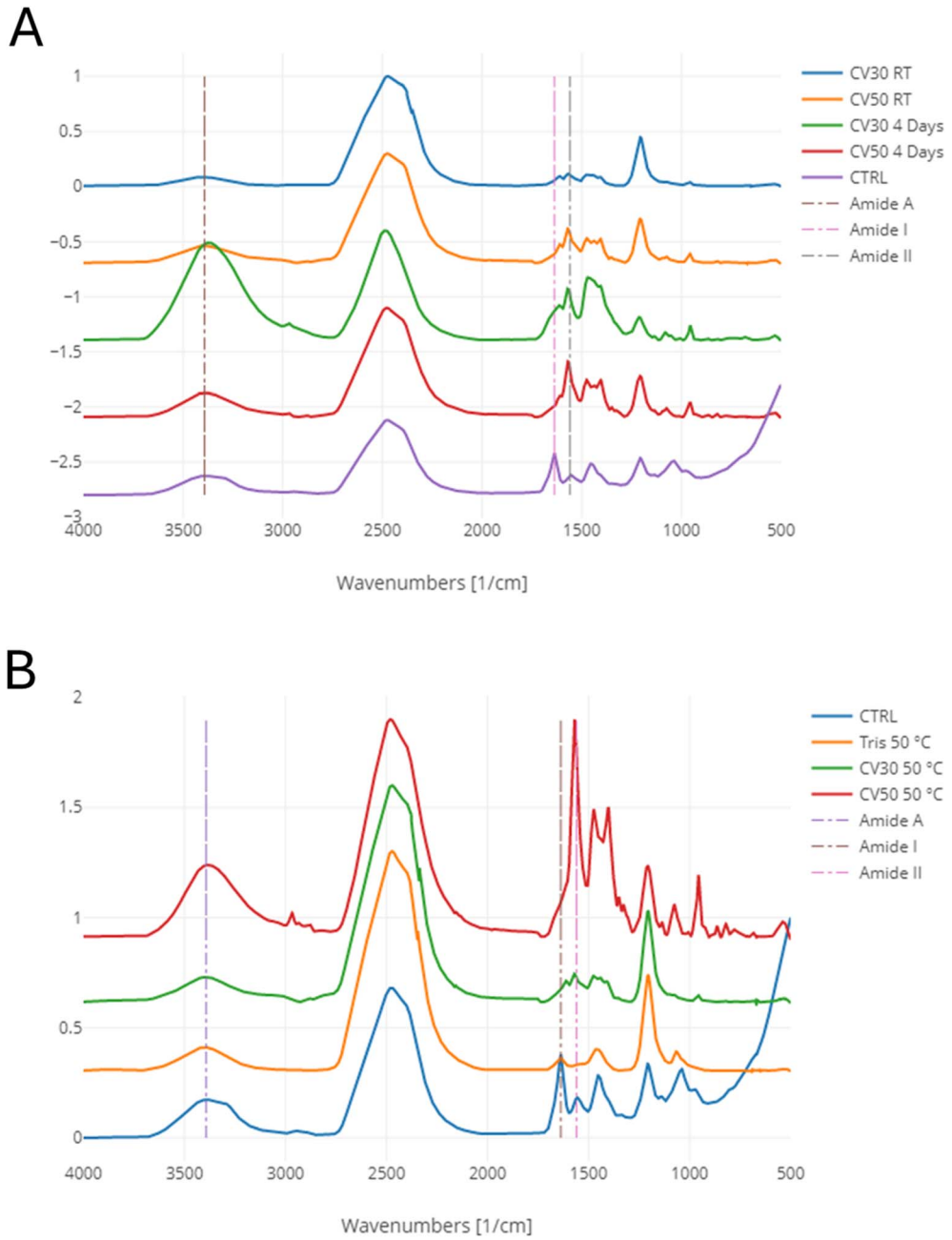

Fig. 9 FTIR Spectra of the antibodies dispersed in D_2O, (A) samples at RT, (B) samples at 50 °C. CTRL: Amab fresh sample serving as a control.

increase in the D_r at 70 °C Amab in Tris buffer. This observation is consistent with prior studies reporting the thermally induced aggregation of IgG in aqueous buffer.[12] Thereby reinforcing the protective efficacy of CV ILs, especially at high temperature (70 °C), with a plausible increase in the melting temperature as previously observed[14] (Table 5 and Fig. 7).

According to Table 6, the AI value of Tris buffer samples displayed a significant increase in AI at 60 °C and 70 °C (AI = 48.98 and 161.4, respectively, at 24 h), indicative of conformational destabilisation and aggregate formation.[12] On the other hand, the CV30 formulation maintained AI values at or below 17, even after 24 hours at 70 °C, whereas the CV50 showed an increase (AI = 24.9), relatively low comparing with tris buffer (161), indicating that it retained its structural integrity under stress. This finding aligns with recent studies demonstrating the thermal resilience of IgG1 antibodies in CV ionic liquids, likely attributed to favourable hydrogen bonding and van der Waals interactions that enhance protein stability.[26–28]

The incubation with CV formations (30 and 50%) at increasing temperature did not cause any notable changes in the λ_{max}. In contrast, samples prepared in Tris buffer and subjected to thermal stress exhibited minor divergence in λ_{max} with a profound hypsochromic effect observed at 70 °C for 24 hours (−6) (Fig. 8).

Table 7 Peak positions of the antibody samples relative to the Amab control sample (fresh sample)

Sample	OH stretching (amide A)	C=O stretching (amide I)	NH bending (amide II)
CTRL	3391 cm^{-1}	1638 cm^{-1}	1566 cm^{-1}
CV30 50	3403 cm^{-1}	1637 cm^{-1}	1568 cm^{-1}
CV50 50	3391 cm^{-1}	1612 cm^{-1}	1568 cm^{-1}
Tris 50	3401 cm^{-1}	1637 cm^{-1}	1539 cm^{-1}
CV30 RT	3404 cm^{-1}	1637 cm^{-1}	1568 cm^{-1}
CV50 RT	3401 cm^{-1}	1615 cm^{-1}	1568 cm^{-1}
CV30 4	3370 cm^{-1}	1639 cm^{-1}	1566 cm^{-1}
CV50 4	3393 cm^{-1}	1615 cm^{-1}	1568 cm^{-1}

Table 8 Average D_r and PDI for CV formulations, after incubation with urea

	3.5 M urea 50 °C		7 M urea 50 °C	
	D_r	PDI	D_r	PDI
CV30	20.1	0.882	17.13	1.00
CV50	28.26	0.859	18.44	1
Tris buffer	11.24	0.83	10.09	0.52

Table 9 Calculated AI for Amab formulations in the presence of urea

	3.5 M urea 50 °C	7 M urea 50 °C
CV30	12	12
CV50	12	14
Tris buffer	11	10

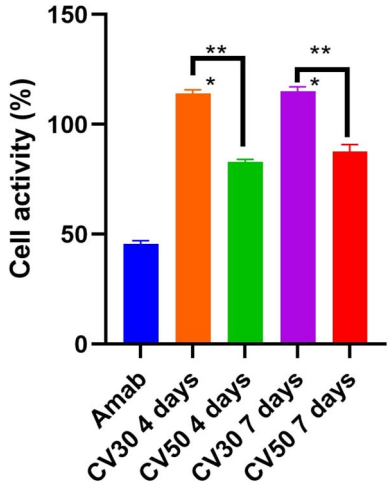

Fig. 10 Cytotoxicity assay (MTT) results using EMT6 cells. EMT6 cells were incubated with various Amab formulations (left at RT) for 4 and 7 days. Statistical difference in comparison to Amab control with *: $p < 0.05$, **: $p < 0.01$, ***: $p < 0.001$. Data represented as mean + SEM ($n = 4$). Amab control: a fresh Amab sample.

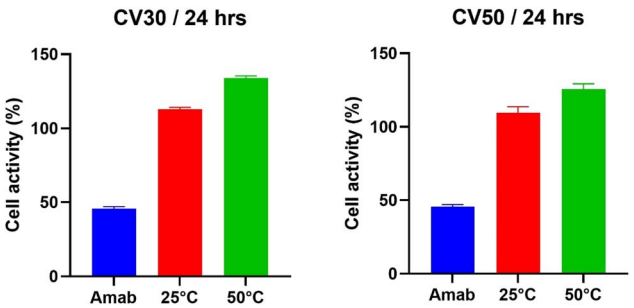

Fig. 11 Cytotoxicity assay (MTT) results using EMT6 cells. EMT6 cells were incubated with various Amab formulations (subjected to thermal stress) for 48 h *, **, ***: statistical difference in comparison to Amab control with a p-value <0.05, <0.01, <0.001. The data represent the mean + SD ($n = 4$). Amab control: a fresh Amab sample referred to as Amab.

3.3 Attenuated total reflectance – Fourier transform infrared spectroscopy

Fig. 9 shows the FTIR spectra of the freeze-dried antibodies following reconstitution in D_2O. The room temperature samples (Fig. 9A) were plotted after 24 hours and 4 days against fresh Amab as a control (CTRL), while the samples incubated at 50 °C are plotted against the CTRL sample, as well as the sample incubated in Tris buffer, which was similarly held at 50 °C.

Peaks characteristic of Amab were identified as the peak at 3391 cm^{-1}, likely representing N–H stretching. The peak at 1638 cm^{-1}, likely representing C=O stretching, and the peak at 1566 cm^{-1}, likely representing NH bending. In a secondary protein structure, the aforementioned peaks are usually associated with amide A, amide I, and amide II, respectively.[29,30] The amide I peak in particular is commonly used to monitor changes in protein secondary structure, and is used to monitor changes in β-sheets as a result of protein unfolding and denaturing.[31,32]

Observing the changes in the spectrum of Amab incubated in Tris buffer at 50 °C, the amide A peak was seen shifted to 3401 cm^{-1}, likely a result of hydrogen bonding with the Tris buffer. The amide II peak exhibited a significant (greater than the 2 cm^{-1} scan resolution) shift to 1539 cm^{-1}, while no significant shift in the amide I peak. The observed shifting suggests both secondary and tertiary structure modifications, likely a result of Amab denaturing at 50 °C. The CV50 sample incubated at 50 °C exhibited shifting in the amide A, likely a result of hydrogen bonding, and another significant shift in the amide I peak, which was seen at 1612 cm^{-1}, with no significant shift in the amide II peak, which is indicative of changes in Amab secondary structure. Similar changes were seen in the FTIR spectra of CV50 samples incubated at room temperature for 24 hours and 4 days, with the amide I peak seen shifted to 1615 cm^{-1} in both samples, suggesting changes to Amab secondary structure (Table 7).

Inversely, samples incubated in CV30 were found to be largely stable; the sample incubated at 50 °C exhibited a shift in amide A peak (3403 cm^{-1}), likely a result of hydrogen bonding with the ionic liquid. No significant shifts, however, were seen

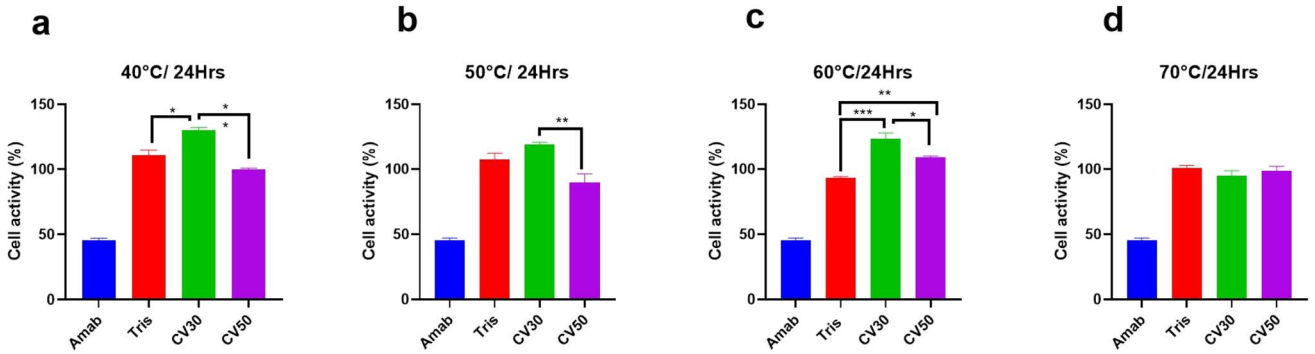

Fig. 12 Cytotoxicity assay (MTT) results using EMT6 cells. EMT6 cells were incubated with various Amab formulations (subjected to thermal stress) for 48 h. *, **, ***: statistical difference in comparison to Amab control with p-values <0.05, <0.01, <0.001. The data represent the mean + SEM ($n = 4$). Amab control: a fresh Amab sample.

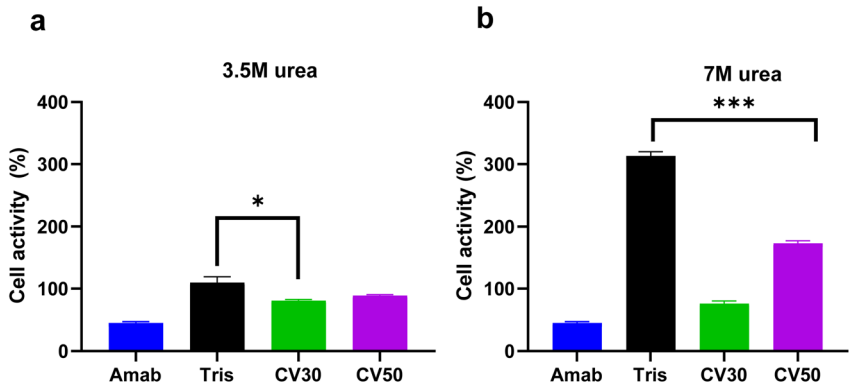

Fig. 13 Cytotoxicity assay (MTT) results using EMT6 cells. EMT6 cells were incubated with Amab formulations (subjected to urea denaturation) for 48 h. *, **, ***: statistical difference in comparison to Amab control with a p-value <0.05, <0.01, <0.001. The data represent the mean + SEM ($n = 4$). Amab control: a fresh Amab sample.

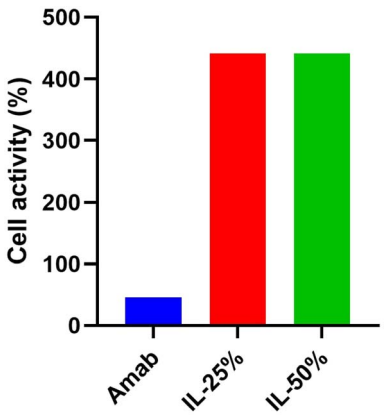

Fig. 14 Cytotoxicity assay (MTT) results using EMT6 cells. EMT6 cells were incubated with IL formulations for 48 h.

in the amide I and amide II peaks, both being observed unshifted at 1637 cm^{-1} and 1568 cm^{-1}, respectively. Similar results were observed in the samples incubated at room temperature for 24 hours and 4 days, with no significant shifts seen in either the amide I or amide II peaks.

The observed results corroborate the findings revealed by DLS and UV spectroscopy, which suggest that IL CV30 has the highest potential of stabilizing Amab.

3.4 Impact of urea-induced stress on Amab stability

Following the identification of CV30 and CV50 as the optimum formulas, we tend to evaluate their ability to reduce chemical denaturation. To this end, following 1 hour of exposure to urea at 50 °C, Amab in CV formulations showed a slight loss in colloidal stability. In the presence of 3.5 M urea, the D_r increased to 20.1 nm in CV30 and 28.26 nm in CV50, with PDI values of 0.882 and 0.859, respectively. Under 7 M urea, the particle size decreased slightly to 17.13 nm and 18.44 nm in CV30 and CV30, but the PDI reached 1.00 in both, indicating a highly polydisperse and aggregated system. In comparison, Tris buffer maintained a more stable colloidal profile. The D_r remained close to 11.24 nm at 3.5 M and 10.09 nm at 7 M, with lower PDI values of 0.83 and 0.52, respectively. This suggests that CV formulation can maintain colloidal stability in the presence of chemical denaturants, such as urea, up to a defined limit without completely preventing it (Table 8 and Fig. S4).

CV30 showed an AI of 12.00 at both urea concentrations, while CV50 increased slightly from 12.00 to 14.00. Tris buffer

maintained lower values of 11.00 and 10.00 at 3.5 M and 7 M, respectively (Table 9 and Fig. S5).

3.5 Cell activity assay

A cytotoxicity assay was conducted to evaluate the biological activity of Amab formulations and to assess the effects of temperature fluctuations and variations in the antibody-to-IL ratio on Amab stability. Cells treated with Amab demonstrated a significant reduction in activity. Conversely, cells exposed to alternative formulations showed a diminished Amab inhibitory effect, as evidenced by elevated cell activity. Such a result aligned with the findings from phase 1 of this project, wherein CV was identified as the optimal formulation for maintaining Amab's structural stability with minimal observed aggregation or degradation; however, it continued to exhibit comparatively lower inhibitory activity than Amab alone.[21]

Formulations containing 50% CV retained higher Amab activity compared to the 30% formulation, regardless of incubation time (Fig. 10). However, this observation could be an assay artefact as the cell activity of the 30% CV was exceeding 100%

In contrast, when incubated for 24 hours at two different temperatures (25 °C and 50 °C), both valine concentrations exhibited similar activity levels. However, cell activity was notably higher at 50 °C, suggesting a loss of Amab stability (Fig. 11). Tris buffer exhibited a relatively similar stabilising effect to that of high valine concentration (50%), regardless of the temperature variation (Fig. 12).

In Fig. 13, it is observed that treatment with a high concentration of urea (7 M) leads to a significant increase in the apparent metabolic activity of the cells. This effect is potentially attributed to the impact of urea on the mitochondrial activity,[33,34] which in turn affects how much MTT is reduced by viable cells. Moreover, valine appears to attenuate the increase in apparent metabolic activity induced by urea in a dose-dependent manner, possibly by interfering with urea's reducing capacity or stabilising Amab against chemical interference.[35]

Unexpectedly, treatment with the IL alone, irrespective of concentration, led to a pronounced increase in cellular activity, which may be attributed to non-specific interactions between the ionic liquid and the MTT reagent or cellular components, potentially resulting in an overestimation of metabolic activity. This was further confirmed when the cells were incubated with IL samples alone (Fig. 14). Consequently, the MTT assay may not be a suitable method for evaluating IL-based formulations. These findings warrant further investigation to confirm the stability and biological activity of the Amab-IL formulation.

4 Conclusion

This research successfully demonstrated choline valinate (CV) could be used as formulation for enhancing the thermal stability of the therapeutic monoclonal antibody, Atezolizumab. The study established that the role of the chemical nature of the amino acid anion, with the valinate anion providing markedly superior protection against thermal aggregation and a possible increase in the melting temperature compared to the glycinate anion and a standard Tris buffer. Formulations containing 30% choline valinate were robust, preserving the monomeric state and structural integrity of the antibody even under severe heat stress, likely due to favourable protein–solvent interactions that shield vulnerable regions of the protein from unfolding. While the ILs successfully mitigated thermal degradation, they were less effective at preventing colloidal instability induced by urea-mediated chemical denaturation, suggesting the addition of excipients in future work. A major limitation of this work, however, was the inability to definitively confirm the preservation of the antibody's biological function. The MTT cytotoxicity assay, chosen for this purpose, proved to be incompatible with the ionic liquid formulations, with an observed significant and artifactual increase in apparent cell activity. This finding renders the biological activity data inconclusive and underscores a critical challenge in the development of IL-based biotherapeutics. Future research must prioritise performing orthogonal MTT assays, such as real-time viability assays, ATP assays, or cell membrane integrity assays, that are not susceptible to such interference. Additionally, reporter gene assays or direct binding assays could effectively demonstrate biological activity. Successfully addressing this step is essential to fully realise the potential of these promising and versatile excipients in the development of next-generation biopharmaceutical formulations with enhanced stability and shelf-life.

Conflicts of interest

There are no conflicts to declare.

Data availability

All the primary results and data generated for this work have been added to the main manuscript or as supplementary information (SI). Supplementary information: Fig. S1–S5. See DOI: https://doi.org/10.1039/d5ra08395h.

Acknowledgements

The authors extend their sincere gratitude to the Deanship of Scientific Research at the University of Petra for their financial support of this study. This research was funded by the Deanship of Scientific Research, University of Petra (grant number 21/4/2023).

References

1 D. Zahavi and L. Weiner, *Antibodies*, 2020, **9**, 34.
2 S. Paul, M. F. Konig, D. M. Pardoll, C. Bettegowda, N. Papadopoulos, K. M. Wright, S. B. Gabelli, M. Ho, A. van Elsas and S. Zhou, *Nat. Rev. Cancer*, 2024, **24**, 399–426.
3 H. Kaplon, A. Chenoweth, S. Crescioli and J. M. Reichert, *mAbs*, 2022, **14**, DOI: 10.1080/19420862.2021.2014296.
4 L. M. Weiner, R. Surana and S. Wang, *Nat. Rev. Immunol.*, 2010, **10**, 317–327.

5 J. Mazieres, A. Rittmeyer, S. Gadgeel, T. Hida, D. R. Gandara, D. L. Cortinovis, F. Barlesi, W. Yu, C. Matheny, M. Ballinger and K. Park, *J. Thorac. Oncol.*, 2021, **16**, 140–150.
6 C. Robert, *Nat. Commun.*, 2020, **11**, 1–3.
7 H. Kaur, *Crit. Rev. Biotechnol.*, 2021, **41**, 692–714.
8 S. Sarvepalli, S. R. Pasika, V. Verma, A. Thumma, S. Bolla, P. K. Nukala, A. Butreddy and P. K. Bolla, *Pharmaceutics*, 2025, **17**, 550.
9 N. B. Pham and W. S. Meng, *Int. J. Pharm.*, 2020, **585**, 119523.
10 T. A. Shmool, L. K. Martin, R. P. Matthews and J. P. Hallett, *JACS Au*, 2022, **2**, 2068–2080.
11 M. Li, R. Zhao, J. Chen, W. Tian, C. Xia, X. Liu, Y. Li, S. Li, H. Sun, T. Shen, W. Ren and L. Sun, *Sci. Rep.*, 2021, **11**, 1–11.
12 A. W. P. Vermeer and W. Norde, *Biophys. J.*, 2000, **78**, 394–404.
13 R. A. Abdulkareem, A. Doekhie, N. Fotaki, F. Koumanov, C. A. Dodson and A. Sartbaeva, *Mol.*, 2024, **29**, 4207.
14 S. Tien and V. Kayser, *Biophys. Rev.*, 2025, **17**, 89–101.
15 S. Sangiorgi, B. Albertini, S. Bertoni and N. Passerini, *Pharmaceutics*, 2025, **17**, 300.
16 M. Reslan and V. Kayser, *Biophys. Rev.*, 2018, **10**, 781–793.
17 N. V. P. Veríssimo, C. U. Mussagy, H. B. S. Bento, J. F. B. Pereira and V. d. C. Santos-Ebinuma, *Biotechnol. Adv.*, 2024, **71**, 108316.
18 A. Tzani, M.-A. Karadendrou, S. Kalafateli, V. Kakokefalou and A. Detsi, *Crystals*, 2022, **12**, 1776.
19 A. Kumar and P. Venkatesu, *Int. J. Biol. Macromol.*, 2014, **63**, 244–253.
20 S. Kirchhecker and D. Esposito, *Curr. Opin. Green Sustainable Chem.*, 2016, **2**, 28–33.
21 B. Alkhawaja, F. Al-Akayleh, Z. Al-Rubaye, G. AlDabet, M. Bustami, M. Smairat, A. S. A. A. Agha, J. Nasereddin, N. Qinna, A. Michael and A. G. Watts, *Int. J. Biol. Macromol.*, 2024, **270**, 132208.
22 D. Dhiman, A. S. C. Marques, M. Bisht, A. P. M. Tavares, M. G. Freire and P. Venkatesu, *Green Chem.*, 2023, **25**, 650–660.
23 Z. Zhang, N. Kang, J. Zhou, X. Li, L. He and H. Sui, *Nanomaterials*, 2019, **9**, 504.
24 D. S. Katayama, R. Nayar, D. K. Chou, J. Campos, J. Cooper, D. G. Vander Velde, L. Villarete, C. P. Liu and M. C. Manning, *J. Pharm. Sci.*, 2005, **94**, 2703–2715.
25 A. Hawe, J. C. Kasper, W. Friess and W. Jiskoot, *Eur. J. Pharm. Sci.*, 2009, **38**, 79–87.
26 D. K. Sahoo, S. Jena, K. D. Tulsiyan, J. Dutta, S. Chakrabarty and H. S. Biswal, *J. Phys. Chem. B*, 2019, **123**, 10100–10109.
27 M. Guncheva, P. Ossowicz, E. Janus, S. Todinova and D. Yancheva, *J. Mol. Liq.*, 2019, **283**, 257–262.
28 X. Li, N. Ma, L. Zhang, G. Ling and P. Zhang, *Int. J. Pharm.*, 2022, **612**, DOI: 10.1016/J.IJPHARM.2021.121366.
29 T. Hayashi and S. Mukamel, *J. Mol. Liq.*, 2008, **141**, 149–154.
30 M. Al-Kelani and N. Buthelezi, *Sking Res. Technol.*, 2024, **30**(6), DOI: 10.1111/srt.13733.
31 D. M. Byler and H. Susi, *Biopolymers*, 1986, **25**, 469–487.
32 Z. Ganim, H. S. Chung, A. W. Smith, L. P. DeFlores, K. C. Jones and A. Tokmakoff, *Acc. Chem. Res.*, 2008, **41**, 432–441.
33 X. Zhao, S. Zhang, M. Wu, B. Zhang, G. Wan, M. Zhang, J. Li, Z. Fei, G. Zhu, S. Jiang, M. Xiao, W. Liu, Z. Zhao, B. Huang and J. Ran, *Metab. Brain Dis.*, 2025, **40**, 186.
34 V. A. Popkov, D. N. Silachev, A. O. Zalevsky, D. B. Zorov and E. Y. Plotnikov, *Int. J. Mol. Sci.*, 2019, **20**, 3094.
35 M. Ghasemi, T. Turnbull, S. Sebastian and I. Kempson, *Int. J. Mol. Sci.*, 2021, **22**, 12827.